PNAS RESEARCH ARTICLE | CELL BIOLOGY OPEN ACCESS

Inflammatory platelet production stimulated by tyrosyl-tRNA synthetase mimicking viral infection

Yosuke Morodomi[a,b,1], Sachiko Kanaji[a,b,1], Brian M. Sullivan[c], Alessandro Zarpellon[d], Jennifer N. Orje[a,d], Eric Won[a,e,f,2], Ryan Shapiro[b], Xiang-Lei Yang[b], Wolfram Ruf[g,h], Paul Schimmel[b,3], Zaverio M. Ruggeri[a,d,3], and Taisuke Kanaji[a,b,3]

Contributed by Paul Schimmel; received July 22, 2022; accepted October 20, 2022; reviewed by Fumihiko Ishikawa and Ellie Tzima

Platelets play a role not only in hemostasis and thrombosis, but also in inflammation and innate immunity. We previously reported that an activated form of tyrosyl-tRNA synthetase (YRS^{ACT}) has an extratranslational activity that enhances megakaryopoiesis and platelet production in mice. Here, we report that YRS^{ACT} mimics inflammatory stress inducing a unique megakaryocyte (MK) population with stem cell (Sca1) and myeloid (F4/80) markers through a mechanism dependent on Toll-like receptor (TLR) activation and type I interferon (IFN-I) signaling. This mimicry of inflammatory stress by YRS^{ACT} was studied in mice infected by lymphocytic choriomeningitis virus (LCMV). Using Sca1/EGFP transgenic mice, we demonstrated that IFN-I induced by YRS^{ACT} or LCMV infection suppressed normal hematopoiesis while activating an alternative pathway of thrombopoiesis. Platelets of inflammatory origin (Sca1/$EGFP^+$) were a relevant proportion of those circulating during recovery from thrombocytopenia. Analysis of these "inflammatory" MKs and platelets suggested their origin in myeloid/MK-biased hematopoietic stem cells (HSCs) that bypassed the classical MK-erythroid progenitor (MEP) pathway to replenish platelets and promote recovery from thrombocytopenia. Notably, inflammatory platelets displayed enhanced agonist-induced activation and procoagulant activities. Moreover, myeloid/MK-biased progenitors and MKs were mobilized from the bone marrow, as evidenced by their presence in the lung microvasculature within fibrin-containing microthrombi. Our results define the function of YRS^{ACT} in platelet generation and contribute to elucidate platelet alterations in number and function during viral infection.

tyrosyl-tRNA synthetase | megakaryocyte | platelet | inflammatory stress | viral infection

Platelets have a primary role controlling hemostasis and vascular integrity (1) but contribute also to inflammation (2, 3), immunity (4, 5), and defense against viral (6–8) and bacterial infections (9, 10). Inflammatory stress alters gene expression in bone marrow megakaryocytes (BM MKs) causing phenotypic changes in generated platelets with pathobiological consequences. Upregulation of integrin alpha 2b (ITGA2B) (integrin αIIb, CD41) during sepsis is linked to increased mortality (11). In contrast, viral infections such as influenza and dengue fever induce type I interferon (IFN-I)-dependent interferon-induced transmembrane protein 3 (IFITM3) expression in MK/platelets facilitating viral suppression (12). The mechanisms that alter MKs and, consequently, platelet functions are yet to be definitively elucidated.

Thrombopoiesis originates from hematopoietic stem cells (HSCs) through common MK-erythroid progenitors maturing to MKs by endomitosis (13–15). An alternative origin is from MK-biased HSCs, a $Lin^-Sca1^+c\text{-}Kit^+$ (LSK) $CD150^+CD48^-CD34^-$ subset of HSCs expressing integrin αIIb (CD41) and von Willebrand factor (VWF) and also known as stem-like MK-committed progenitors (SL-MkPs) (16–19). These bypass the MEP stage and generate platelets in mice treated with polyinosinic:polycytidylic acid (17). In blood, platelets from the MEP pathway or MK-biased HSCs are not easily distinguished; thus the induction of these cells and functional consequences in pathophysiological conditions are still debated.

Eukaryote aminoacyl-tRNA synthetases (aaRSs) have acquired noncanonical activities beyond translation (20–22). In insects, tyrosyl-tRNA synthetase (YRS) incorporated Glu-Leu-Arg (ELR) and endothelial monocyte-activating polypeptide II (EMAP-II) motifs contributing extranslational functions (23) upon activation by stress (24). We recently reported that a gain-of-function mutation (Y341A) activates recombinant YRS (YRS^{ACT}) and accelerates recovery from thrombocytopenia in mice by inducing thrombopoiesis from MKs expressing markers of stem cells (Sca1) and monocyte/macrophages (F4/80) (25). More recently, we utilized YRS^{ACT} prepared by truncation after residue 377 in the EMAP-II domain, which had improved protein stability (26). Using the latter form of YRS^{ACT}, here we show it activates Toll-like receptor (TLR) 7 inducing an alternative pathway of

Significance

Infection is often associated with thrombocytopenia and rapid replenishment of platelets may be important to maintain vascular homeostasis. We found that an activated form of tyrosyl-tRNA synthetase (YRS^{ACT}) mimics inflammatory stress in mice, inducing a distinct population of megakaryocytes (MKs) from myeloid/MK-biased hematopoietic stem cells bypassing the classical MK-erythroid progenitor (MEP) pathway. In mice infected by lymphocytic choriomeningitis virus, myeloid/MK progenitors and MKs were mobilized from the bone marrow into the circulation and found trapped in the lung microvasculature within fibrin containing microthrombi. These findings define the role of YRS^{ACT} in platelet generation and advance our understanding of functionally distinct alternative platelet production during viral infection.

Competing interest statement: Z.M.R. is Founder, President, and CEO, W.R. is Member of the Board, A.Z. is Chief Innovation Officer of MERU-VasImmune, Inc.; all have equity interest in the Company. S.K. and T.K. have equity interest in MERU-VasImmune, Inc., and J.N.O. is an employee of the company. X.-L.Y. and P.S. have financial interest in aTyr Pharma. aTyr works on therapeutic applications of tRNA synthetases and MERU VasImmune works on hematological tests. Neither aTyr Pharma nor MERU have any financial interest or intellectual property rights associated with the current work. The remaining authors declare no competing financial interests. Ellie Tzima, one of the reviewers, has financial interest in aTyr Pharma, but no interest specifically in this work.

[1]Y.M. and S.K. contributed equally to this work.

[2]Present address: Children's Hospital of Orange County, Orange, CA.

[3]To whom correspondence may be addressed. Email: schimmel@scripps.edu, ruggeri@scripps.edu, or tkana@scripps.edu.

This article contains supporting information online at https://www.pnas.org/lookup/suppl/doi:10.1073/pnas.2212659119/-/DCSupplemental.

Published November 21, 2022.

thrombopoiesis through IFN-I-dependent mechanisms as seen during viral infection or after TLR4 activation by bacterial lipopolysaccharide (LPS). TLR7-induced inflammatory MKs and platelets have enhanced susceptibility to activation that may not only contribute to hemostasis but also increase thrombotic risk. These findings may advance our ability to monitor hemostatic function and prevent bleeding as well as thrombotic complications associated with severe infections and inflammatory stress.

Results

YRS^{ACT} Influences Thrombopoiesis through IFN-I Signaling. Unlike cultured BM cells from wild-type C57BL/6 (WT) mice (25), those from IFN α/β receptor-deficient (IFNAR$^{-/-}$) mice failed to expand Sca1$^+$F4/80$^+$ MKs after YRS^{ACT} treatment (Fig. 1*A*). Of note, in transgenic mice expressing Enhanced Green Fluorescent Protein (EGFP) under Sca1 transcriptional regulation (27), YRS^{ACT} injection increased Sca1/EGFP$^+$ blood platelets from negligible to ~20% of total. However, <1% platelets but >50% CD41$^+$ BM cells bound anti-Sca1 antibody (Fig. 1 *B*–*D*), indicating platelets, unlike MKs, lack Sca1 on the cell surface. MKs expressing cluster of differentiation 41 (CD41) (integrin αIIb) and CD42b (GPIbα) were present in both Sca1/EGFP – and + BM cells of Sca1/EGFP Tg mice, but only the latter expressed F4/80 alongside CD42b (Fig. 1 *E*–*G*).

Transcriptome analysis of CD41$^+$CD42b$^+$ MKs showed that the Sca1/EGFP$^-$ group had greater erythroid than myeloid gene expression, as expected of "normal" MKs from the MEP pathway; in contrast, the Sca1/EGFP$^+$ group had the opposite higher expression of myeloid than erythroid genes, as well as higher expression of stem cell-related genes (Fig. 2*A*). These latter findings are consistent with "inflammatory" MKs from myeloid/MK-biased HSCs, as also shown by high levels of IFN-I-induced Ifitm 1/2/3 (12). To confirm the conclusion excluding off-target effects of the Sca1/EGFP transgene, we performed multidimensional flow cytometric analysis of wild type (WT) BM cells. We identified two populations of CD41$^+$CD42b$^+$ MKs (Fig. 2 *B* and *C*), one (MK#1) with greater stem cell and myeloid gene expression than the other (MK#2), thus confirming the results in to Sca1$^+$ and Sca1$^-$ MKs, respectively, of Sca1/EGFP Tg mice.

YRS^{ACT} Induction of TLR/IFN-I Signaling Mimics Viral and Bacterial Infections. We previously reported thrombopoietic activities of YRS^{ACT} mediated by TLRs (25). Thus, we tested whether LPS, which activates TLR4 as in bacterial infection (29), and Gardiquimod (GDQ), which activates TLR7 (30) as in viral infection (31), can influence thrombopoiesis-like YRS^{ACT}. For this purpose, we crossed Sca1/EGFP Tg and IFNAR$^{-/-}$ mice to generate Sca1/EGFP – or + BM cells that were IFNAR$^-$. Ex vivo, unstimulated IFNAR$^+$ BM cell cultures contained ~50:50 Sca1/EGFP – and + MKs and precursors, while IFNAR$^-$ BM cell cultures had less than half as many, nearly all Sca1/EGFP$^-$ (Fig. 3*A*). In IFNAR$^+$ BM cell cultures, treatment with LPS or GDQ significantly decreased Sca1/EGFP$^-$ and increased Sca1/EGFP$^+$ MKs and precursors; in IFNAR$^-$ cultures, LPS significantly increased Sca1/EGFP$^-$ but not Sca1/

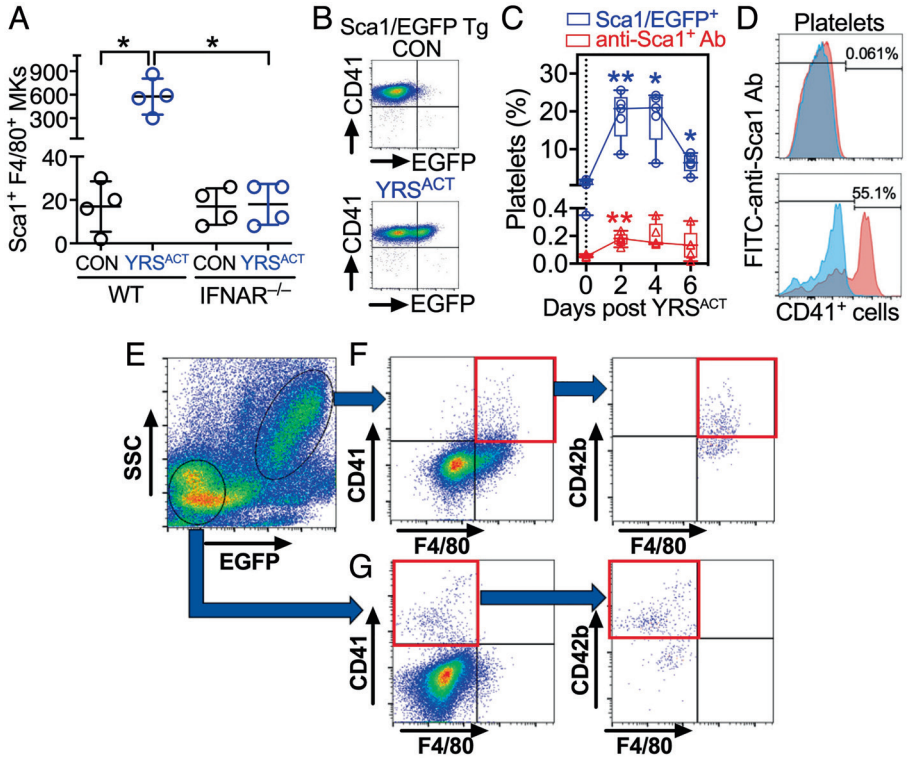

Fig. 1. Characterization of Sca1/EGFP$^+$ MKs and platelets. (*A*) BM cells from WT or IFNAR$^{-/-}$ mice were cultured with 200 nM YRS^{ACT} or vehicle control (CON). After 3 d, CD41$^+$ cells costained by anti-Sca1 and anti-F4/80 antibodies were enumerated by flow cytometry (Sca1$^+$F4/80$^+$ MKs). Data are shown as scatter plots with mean ± SD (n = 4). (*B*) Flow cytometry of blood platelets from Sca1/EGFP Tg mice treated with 30-mg/kg intravenous YRS^{ACT} or CON. (*C*) Percentage of blood platelets from the above mice showing green fluorescence (Sca1/EGFP$^+$; blue) or anti-Sca1 binding (red) measured at indicated times after treatment. Data (n = 5), shown as 25th–75th percentile boxes with min-to-max whiskers, were analyzed by (*A*) Brown-Forsythe/Welch one-way ANOVA with Dunnett's T3 posttest for paired comparisons; or (*C*) repeated measures (RM) two-way ANOVA without assuming sphericity (Geisser–Greenhouse correction) with Dunnett's posttest for before–after comparisons. *P <0.05, **P <0.01. (*D*) Anti-Sca1 antibody binding is negligible in blood platelets (*Top*), but present in >50% CD41$^+$ BM cells (*Bottom*). (*E*) BM cells from Sca1/EGFP Tg mice gated as Sca1/EGFP − or + by flow cytometry (circled, *Bottom Left* or *Upper Right*, respectively). (*F*) Sca1/EGFP$^+$ cells included CD41$^+$, F4/80$^+$ and CD41$^+$F4/80$^+$ (double-positive) cells (*Left*); ~half of the latter was also CD42b$^+$ (*Right*). (*G*) Sca1/EGFP$^-$ cells included CD41$^+$ and F4/80$^+$ cells, but double-positive cells were negligible (*Left*); over half of the CD41$^+$ cells was also CD42b$^+$ (*Right*).

A

Categories	Genes	TPM Sca1/EGFP⁺ MKs	TPM Sca1/EGFP⁻ MKs
MK	Pf4	11181.9	198.6
	Itga2b	1010.5	101.7
	Gp5	429.5	67.6
	Gp1bb	321.8	46.9
	Mpl	392.7	29.0
	Gp9	234.8	108.2
	Etv6	132.9	15.3
	Gp1ba	102.3	39.6
	Vwf	89.3	11.1
Stem cell	Cd34	113.6	0.2
	Kit	77.3	10.0
Erytroid	Epor	53.0	232.5
	Band3	43.9	3222.7
	Glycophorin A	43.3	2618.3
	Tfrc	35.6	633.3
Myeloid	Mpo	7851.9	9.2
	Elastase	4809.8	11.3
	Cathepsin G	1218.2	6.0
	Apoe	559.3	28.0
	Ms4a3	453.6	0.4
IFN stimulated gene	Ifitm3	1498.2	370.6
	Ifitm2	1028.2	103.9
	Ifitm1	90.6	17.7

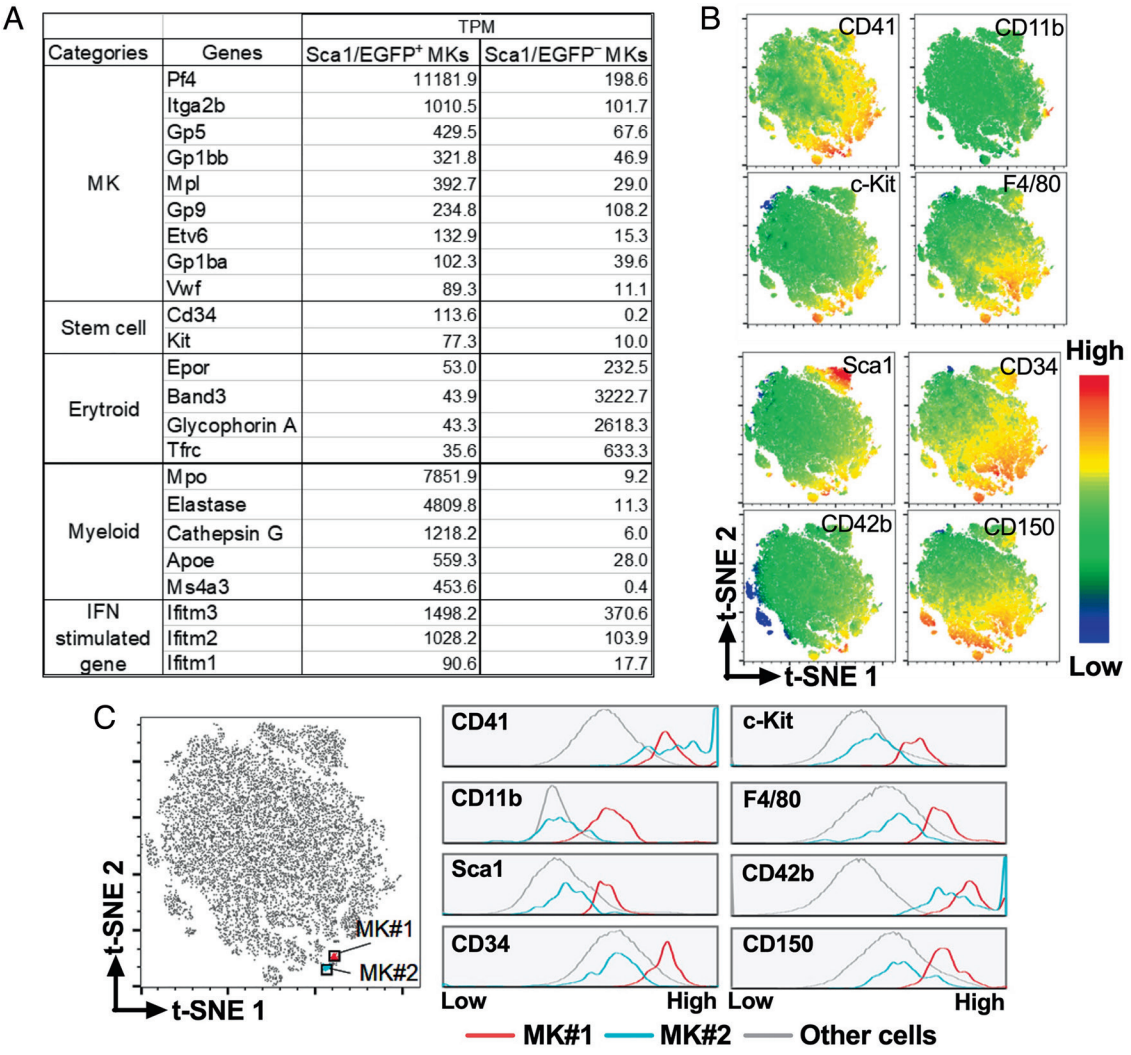

Fig. 2. MK analysis by RNA-Seq and high-dimensional mass cytometry with t-distributed stochastic neighbor embedding (t-SNE). (*A*) Gene expression differences in two MK populations sorted from Sca1/EGFP Tg mouse BM cells on the basis of Sca1/EGFP expression. Values are shown as Transcripts Per kilobase Million (TPM). (*B*) BM cells from WT mice with 2N/4N DNA content were analyzed by flow cytometry and characterized for surface expression of stem cell markers CD34, Sca1, CD117 (c-Kit), and CD150 (SLAMF1); MK markers CD41 (integrin αIIb) and CD42b (GPIbα); and granulocyte/monocyte markers CD11b (integrin αM) and F4/80. The multidimensional data were analyzed by t-SNE (28) showing expression of each marker with color-coded intensity. (*C*) The t-SNE plot on the left identifies two subsets of cells (MK#1 and MK#2) expressing comparable levels of the MK/platelet markers CD42b and CD41; the histograms on the right show expression levels of the indicated markers in MK#1, MK#2 and all other cells. Prevalence of stem cell and myeloid markers differentiates "inflammatory" MK#1 from "normal" MK#2.

EGFP⁺ MKs and precursors, while GDQ increased only the latter, albeit with numbers remaining very low (Fig. 3*A*).

In vivo, unstimulated mouse IFNAR⁺ BM had ~50:50 Sca1/EGFP + and – MKs and precursors; IFNAR⁻ BM had similar total numbers of these cells, but nearly all Sca1/EGFP⁻ (Fig. 3*B*). At day two posttreatment of IFNAR⁺ mice, LPS significantly decreased Sca1/EGFP⁻ and GDQ significantly increased Sca1/EGFP⁺ MKs and precursors in the BM; in IFNAR⁻, as in IFNAR⁺, LPS significantly decreased Sca1/EGFP⁻ MKs and precursors; GDQ had no effect (Fig. 3*B*). Thus, TLR4 activation negatively regulates Sca1/EGFP⁻ MK development (normal thrombopoiesis) in vivo irrespective of IFNAR, but IFN-I signaling is required for the expansion of Sca1/EGFP⁺ inflammatory MKs. Supporting this conclusion, LPS and GDQ significantly increased the number of high-ploidy (8-16n) Sca1/EGFP⁺ MKs in IFNAR⁺ cultures ex vivo, but much fewer developed in IFNAR⁻ cultures and only after stimulation by GDQ (*SI Appendix*, Fig. S1*A*). Notably, 16–32n MKs were significantly induced in vivo only by GDQ stimulation in IFNAR⁺ mice, with >10 times lower numbers in IFNAR⁻ mice (*SI Appendix*, Fig. S1*B*). Consistent with interferon alpha/beta receptor (IFNAR) involvement in these processes, four IFN-I gene transcripts were variably up-regulated in mice treated with LPS or GDQ (*SI Appendix*, Fig. S2).

To evaluate further the balance between suppression (32–35) and stimulation (36) of BM function involving IFN-I, we measured total and Sca1/EGFP – or + platelets in mice before and for 7 d after LPS or GDQ administration. A single injection of LPS, but not GDQ, severely reduced total blood platelets, which reached the lowest counts in 2–4 d and fully recovered in 7 d; within this timeframe, both treatments significantly reduced Sca1/EGFP⁻ and increased the initially absent Sca1/EGFP⁺ platelets; both eventually returned to their respective pretreatment levels (Fig. 3*C*). Notably, at the lowest point of Sca1/EGFP⁻ platelet depletion, the percentage of Sca1/EGFP⁺ platelets in blood was similar (~50%) after both treatments; in absolute numbers; however, ~3 times more Sca1/EGFP⁺ platelets were generated after GDQ (involving TLR7) than LPS (involving TLR4) stimulation (Fig. 3*C*). Thus, the loss of Sca1/EGFP⁻ platelets was fully compensated in the former but not the latter condition. In untreated mice, the majority of CD41⁺ cells comprising MKs and committed MK progenitors in the BM were Sca1/EGFP⁻ or only

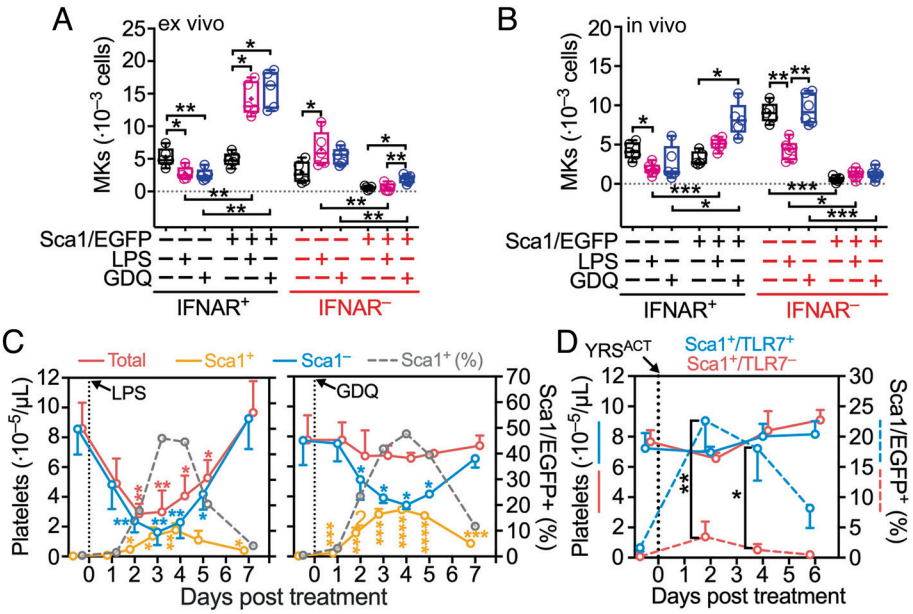

Fig. 3. TLR4 and TLR7 activation variably inhibits normal and induces inflammatory platelet generation through IFNAR signaling. (*A*) Quantification of Sca1/EGFP − or + MKs in BM cells ($1.5 \cdot 10^7$) from IFNAR + or − Sca1/EGFP Tg mice after 3 d in culture with GDQ (0.5 μg/mL), LPS (1 μg/mL), or vehicle control (CON). (*B*) Analysis (as in *A*) of BM cells harvested from the right femur of IFNAR + or − Sca1/EGFP Tg mice 2 d after intraperitoneal (i.p.) injection of GDQ (1 mg/kg) or LPS (2 mg/kg). Data in (*A* and *B*)—shown as 25th–75th percentile boxes with min-to-max-whiskers and individual values (n = 5)—were analyzed by Brown–Forsythe and Welch one-way ANOVA with Dunnett's T3 posttest for multiple paired comparisons. (*C*) Platelets in blood were monitored in Sca1/EGFP Tg mice before and for 7 d after treatment with GDQ or LPS as in (*B*). Platelets were enumerated with a blood cell counter (Procyte Dx) and the percentage of Sca1/EGFP$^+$ was determined by flow cytometry, from which numbers of Sca1/EGFP$^+$ and Sca1/EGFP$^-$ platelets were calculated. Data shown as mean ± SD (n = 5 in each group) were analyzed by RM two-way ANOVA with Geisser–Greenhouse correction and Dunnett's posttest (see Fig. 1*C*). (*D*) Total counts (solid lines) and percentage of Sca1/EGFP$^+$ platelets (broken lines) monitored in TLR7$^{+/+}$ (blue lines) or TLR7$^{-/-}$ (red lines) Sca1/EGFP Tg mice before and for 6 d after a single intravenous injection of YRS^{ACT} (30 mg/kg; n = 4 in each group). Data shown and analyzed as in (*C*), except that Šídák's posttest was used. Only significant differences are indicated: **P* <0.05, ***P* <0.01, ****P* <0.001, *****P* <0.0001.

weakly expressed Sca1/EGFP; after GDQ treatment, most CD41$^+$ cells in the BM were Sca1/EGFP$^+$ (*SI Appendix*, Fig. S3).

These findings and the absence of severe thrombocytopenia in mice treated with YRS^{ACT} (25), similar to GDQ as shown here, suggested that YRS^{ACT} might activate TLR7 to induce inflammatory thrombopoiesis. To test this hypothesis, we crossed Sca1/EGFP Tg with TLR7$^{-/-}$ mice to generate a strain with Sca1/EGFP$^+$TLR7$^-$ MKs and platelets. For 6 d after YRS^{ACT} injection, blood platelet counts remained similar in TLR7 + or – mice (Fig. 3*D*, blue or red solid line, respectively); however, the percentage of Sca1/EGFP$^+$ platelets became significantly, albeit transiently, higher in TLR7 + than – mice (Fig. 3*D*, blue or red broken line, respectively). Thus, similar to GDQ, YRS^{ACT}, through TLR7 activation and IFNAR signaling, may partially compensate inefficient platelet production by the induction of inflammatory thrombopoiesis.

Functional Differences between Normal and Inflammatory Platelets. For these studies, we analyzed blood from Sca1/EGFP Tg mice before (control) and 3 d after GDQ injection, which markedly increases Sca1/EGFP$^+$ platelets in blood. By transcriptome analysis, Sca1/EGFP$^+$ platelets of GDQ-treated mice had increased the expression of a number of genes compared with Sca1/EGFP$^-$ platelets of control mice, including Sca1 (Ly6a) and those relevant for platelet function (*SI Appendix*, Fig. S4). Phenotypically, membrane CD41 (integrin αIIb) and intracellular filamin A were significantly higher in Sca1/EGFP + than – platelets of GDQ-treated mice, but both were significantly lower in Sca1/EGFP$^-$ platelets of treated than control mice (Fig. 4 *A* and *B*; note that mice not exposed to GDQ lacked Sca1/EGFP$^+$ platelets in blood). Moreover, fibrinogen bound significantly more to adenosine diphosphate (ADP)-stimulated Sca1/EGFP + than – platelets from GDQ-treated mice, but significantly less to Sca1/EGFP$^-$ platelets of GDQ-treated than control mice (Fig. 4 *C* and *D*, *Left*), mirroring membrane levels of CD41 (see Fig. 4*A*), part of the fibrinogen receptor. No changes in fibrinogen binding were detectable when Sca1/EGFP + and – platelets were not evaluated separately (Fig. 4 *D*, *Right*). Unlike fibrinogen, annexin V binding induced by alborhagin, a GPVI agonist (37), was not significantly different from Sca1/EGFP + and – platelets of GDQ-treated mice, but both bound significantly more than Sca1/EGFP$^-$ platelets of control mice (Fig. 4 *E* and *F*, *Left*). This difference was detectable also without separating platelets for Sca1/EGFP expression (Fig. 4 *F*, *Right*).

To investigate further the origin of inflammatory MKs, we first demonstrated that MKs developing in Sca1/EGFP$^+$ BM cell cultures supplemented with GDQ or thrombopoietin were morphologically distinct, the former being more tightly adherent and with focal CD11b staining (*SI Appendix*, Fig. S5*A*). We then harvested BM cells of Sca1/EGFP Tg mice 17 h after administration of GDQ or vehicle control and separated Sca1/EGFP$^+$ CD41$^+$ progenitors from more mature MKs (*SI Appendix*, Fig. S5*B*) to perform bulk RNA-Seq analysis. The results (*SI Appendix*, Fig. S5*C*) showed that control Sca1/EGFP$^+$ CD41$^+$ progenitors expressed stem cell markers (e.g., CD150, CD34), a marker for granulocyte–monocyte progenitors (Ms4a3), and myeloid markers (e.g., CD11b, myeloperoxidase (MPO)) (*SI Appendix*, Fig. S5*C*). These cells also express VWF, but little or none of the mature MK markers (e.g., GPIbα, GPVI), indicating enrichment in myeloid/MK-biased progenitors. GDQ administration notably enhanced myeloid along with IFN-stimulated genes (Ifitm2, Ifitm3, Ifit2, and Ly6a), while decreasing stem cell markers other than Ly6a. Such findings support the conclusion that the pool of Sca1/EGFP$^+$ CD41$^+$ cells is enriched in myeloid/MK-biased progenitors, and treatment with GDQ promotes differentiation toward myeloid lineage. Of note, CD41 mRNA is decreased in GDQ-treated

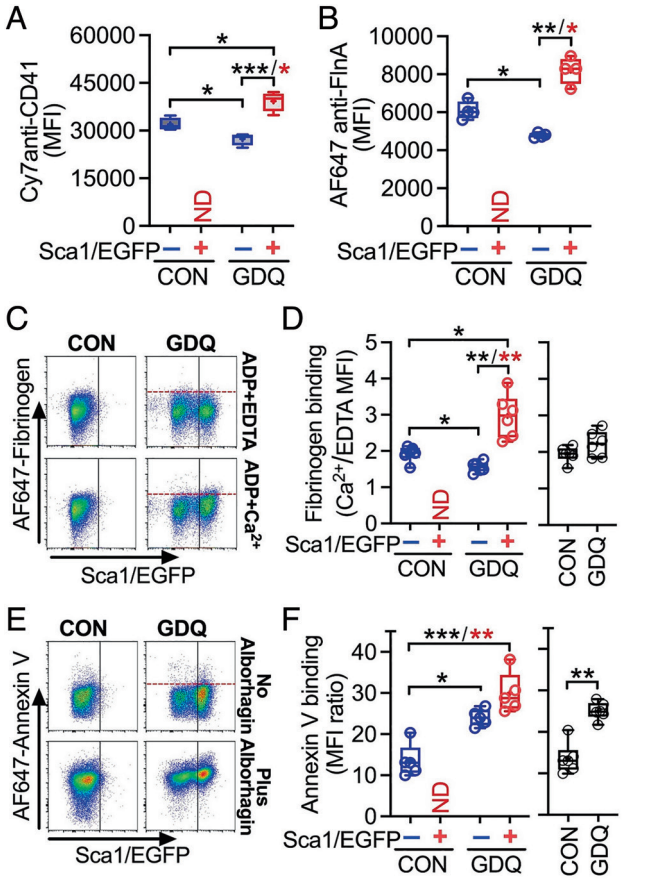

Fig. 4. Functional characterization of Sca1/EGFP$^{+/-}$ platelets. Blood cells collected from Sca1/EGFP Tg mice 3 d after GDQ or CON injection were permeabilized, fixed, and stained with antibodies against (*A*) PE-Cy7-labeled anti-CD41; or (*B*) AF647-labeled anti-filamin A. The median fluorescence intensity (MFI) of bound antibody was taken to represent levels of the cognate antigen. (*C*) Blood from mice treated with GDQ or CON was diluted in Tyrode's buffer (1.5–100 µL final), to which AF647-fibrinogen (15 µg/mL) was added with 0.2 mM Ca^{2+} or 2 mM EDTA (negative control) and 10 µM ADP to activate platelets at room temperature. After 10 min, AF405-anti-mouse GPIbα MoAb (5A7) was added (to identify platelets) and fibrinogen binding to Sca1/EGFP + or − platelets was separately evaluated. (*D*, *Left* panel) Bound fibrinogen calculated as the ratio of AF647 MFI values on platelets with added Ca^{2+} or EDTA; ND indicates no Sca1/EGFP^{+} platelets detected in untreated mice. (*D*, *Right* panel) Fibrinogen bound to all platelets without gating for EGFP fluorescence. (*E*) Evaluation of AF647-Annexin V binding to blood platelets in the presence of 3 mM Ca^{2+} and 200 nM apixaban (FXa inhibitor to prevent coagulation) with or without the addition of the platelet GPVI agonist, Alborhagin (2.5 µg/mL). For additional details, see panel (*C*). (*F*, *Left* and *Right*) AF647-Annexin V binding to platelets measured with the same method as fibrinogen in (*D*, *Left* and *Right*). Data in (*A*, *B*, *D*, and *F*) are shown as 25th–75th percentile boxes with min-to-max-whiskers and individual values (n = 4 and 6, respectively). Statistical analysis was performed by RM one-way ANOVA with Geisser–Greenhouse correction and Tukey's posttest for paired comparisons (black asterisks) or nonparametric Friedman test followed by Dunn's posttest (red asterisks), except for data in *D*, *F*, *Right* panel, analyzed by two-tailed paired *t* test. **P* <0.05, ***P* <0.01, ****P* <0.001.

Sca1/EGFP^{+} progenitors while protein expression is slightly increased (1.2-fold), which is in line with the previous report that inflammation-mediated MK-protein expression in SL-MkPs is regulated by posttranscriptional mechanisms (17).

YRS and Viral Infection Induce Inflammatory Thrombopoiesis through a Common TLR Pathway. Our results show that TLR4 and TLR7 initiate IFNAR-mediated signaling that induces alternative thrombopoiesis, as does YRS^{ACT} through TLR7. Sensing viral-associated pathogen patterns, specifically single-stranded RNA, is a TLR7 function (31,38–40). Thus, we studied how thrombopoiesis is affected during infection by two different strains of lymphocytic choriomeningitis virus, a single-stranded RNA arenavirus (41): Armstrong (LCMV-A) and Clone 13 (LCMV-13) causing acute and chronic infection, respectively.

In agreement with previous findings (42), platelet counts dropped but recovered quickly in mice infected by LCMV-A, with lowest values ~5 d and complete recovery ~15 d postinfection (Fig. 5 *A*, *Top*). Thrombocytopenia caused by LCMV-13 persisted for ~10 d and recovery was complete in ~20 d (Fig. 5 *A*, *Bottom*). In both conditions, Sca1/EGFP^{-} platelets dropped as thrombocytopenia developed, but in sharp contrast Sca1/EGFP^{+} platelets increased from near zero before infection to >80% of total when thrombocytopenia was at the lowest levels (Fig. 5 *A*, *Top* and *Bottom*; gray broken lines). This alone maintained platelets above the level required to prevent life-threatening hemorrhage (42). In LCMV-A-infected mice, recovery from thrombocytopenia depended on increasing Sca1/EGFP^{-} platelets, as Sca1/EGFP^{+} platelets inversely decreased and became undetectable by the time platelet counts normalized (Fig. 5 *A*, *Top*). Sca1/EGFP^{-} platelets also increased during recovery from thrombocytopenia in LCMV-13-infected mice, but Sca1/EGFP^{+} platelets remarkably kept circulating, albeit in slowly decreasing proportion that stabilized at ~50% by the time platelet counts normalized (Fig. 5 *A*, *Bottom*). In the BM, Sca1/EGFP – and + MKs were nearly equal in number before infection by LCMV-A, but the former decreased and the latter increased on days 3 and 7 after infection, returning toward equivalence by day 16 (Fig. 5*B*). Consistent with efficient Sca1/EGFP^{+} platelet production, Sca1/EGFP^{+} MKs in the BM had high ploidy (*SI Appendix*, Fig. S6).

Blood of Sca1/EGFP Tg mice contained CD41^{+} cells—including hematopoietic progenitors (43,44), MKs, and myeloid-biased progenitors (45)—distinguished from platelets by staining with deep red anthraquinone 5 (DRAQ5), a nuclear dye (Fig. 5*C*). Before infection, these cells were Sca1/EGFP – and + in nearly equal proportion (Fig. 5 *D*, *Top* and *Bottom*); between 1 and 3–5 d after infection by LCMV-A or LCMV-13, both Sca1/EGFP – and + components of CD41^{+} cells decreased, then increased rapidly to a maximum ~7 d postinfection; at this point >90% were Sca1/EGFP^{+} (Fig. 5 *D*, *Top* and *Bottom*). Thereafter, these cells decreased progressively toward preinfection numbers, but the preponderance of Sca1/EGFP^{+} cells persisted as clearly seen in LCMV-13-infected mice (Fig. 5 *D*, *Bottom*). Imaging flow cytometry showed these CD41^{+} cells had variable sizes and contained subsets of CD11b^{+} as well as DRAQ5^{+}/Sca1^{+}/CD41^{+}/CD42b (GPIbα)$^{+}$ cells, the latter corresponded to circulating Sca1^{+} mature MKs (*SI Appendix*, Fig. S7 *A* and *B*). Of note, the lungs of noninfected Sca1/EGFP Tg mice contained CD41^{+} cells and platelets with minimal fibrin; 7 d after LCMV-A infection, CD41^{+} cells with aggregated platelets and fibrin increased markedly (*SI Appendix*, Fig. S7*C*).

Plasma YRS Increases during Viral Infection. YRS displays cytokine activities after secretion from cells and proteolytic cleavage (24,46). Accordingly, we previously reported that YRS secreted into plasma is promptly cleaved by matrix metalloproteases and elastase, after which it may contribute to immune cell activation (26). In the present study, we found that plasma YRS levels were significantly increased in mice chronically infected by LCMV-13, with higher than preinfection values persisting for several weeks (Fig. 6). Although changes in the post/preinfection ratio in circulating blood were relatively modest at ~1.25-2, concentrations are likely to increase more in target organs where biological activity is exerted. It remains to be clarified which cells are the source of enhanced YRS secretion during inflammation. It has been previously reported that YRS is secreted from apoptotic cells (24). During LCMV-13 infection, viral replication occurs

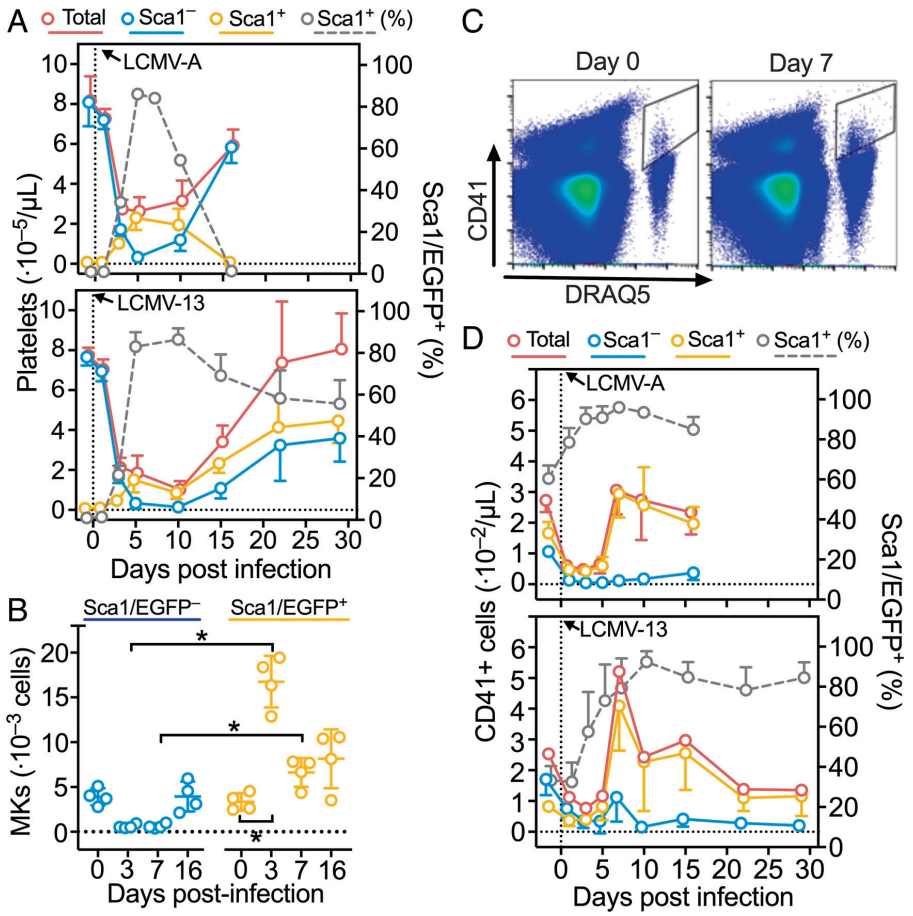

Fig. 5. Inflammatory thrombopoiesis in mice infected by LCMV. (*A*) Total platelet count (red solid line) and percentage of Sca1/EGFP$^+$ platelets (gray broken line) measured before and after injection of LCMV-A (*Upper* panel) or LCMV-13 (*Lower* panel) into Sca1/EGFP Tg mice. From these two values, the number of Sca1/EGFP$^-$ and Sca1/EGFP$^+$ platelets was calculated (blue and orange lines, respectively). Data shown as mean ± SD (*Upper* panel: n = 10, except n = 5 for day 16 excluded from statistical evaluation, *Lower* panel: n = 5). (*B*) BM cells were harvested from femurs of Sca1/EGFP Tg mice at the indicated days after LCMV-A infection and the number of MKs was determined by flow cytometry. Data (n = 4) shown as scatter plots with mean ± SD, were analyzed by RM one-way ANOVA with Geisser–Greenhouse correction and with Šídák's posttest for multiple paired comparisons. (*C*) Flow cytometric analysis of blood cells from WT mice stained with anti-CD41 antibody and DRAQ5 in the presence of 2 mM EDTA before and 7 d after infection with LCMV-A. (*D*) Number of CD41$^+$ nucleated cells and percentage of Sca1/EGFP$^+$ measured in blood of Sca1/EGFP Tg mice before and after infection with LCMV-A (*Upper* panel) or LCMV-13 (*Lower* panel). Data, shown as mean ± SD, were analyzed as in (*A*). *P <0.05.

in pulmonary endothelial cells, which are targeted by cytotoxic T lymphocytes. Thus, we speculate that such stressed cells are the source of enhanced YRS secretion during LCMV-13 infection. Additionally, we have previously reported that platelets uptake YRS in the plasma and store it inside cells, which can be released upon activation (26). Therefore, it is also possible that blood cells including platelets are also contributing to enhanced YRS secretion during inflammation.

Discussion

We show here that YRS^{ACT} activates TLR7 to induce inflammatory platelet generation from MK-biased HSCs (25), a mechanism limiting the severity of thrombocytopenia during viral infections, thus risk of bleeding and endothelial dysfunction (42). Using Sca1 expression to discriminate between inflammatory and normal platelets, we demonstrate that TLR7 and IFNAR are required for generating Sca1$^+$ inflammatory platelets. Since MyD88$^{-/-}$ mice are insensitive to YRS^{ACT} influence on thrombopoiesis (25), this defines the role of TLR7/MyD88/IFN-I signaling in the induction of inflammatory platelets (Fig. 7). TLR4 may also contribute to this mechanism (25). Using LPS and GDQ to activate TLR4 and TLR7, respectively (29,30), we also show how these TLRs distinctly influence normal and inflammatory platelet production (Fig. 7).

In previous work, the subset of MKs expanded by YRS^{ACT} was recognized by anti-Sca1 antibody binding (25). Here, using Sca1/EGFP Tg mice (27), we confirm that inflammatory MKs express Sca1 and Sca1/EGFP transgene, but, unlike their progenitors, platelets have no surface Sca1, and Sca1/EGFP serves as a useful

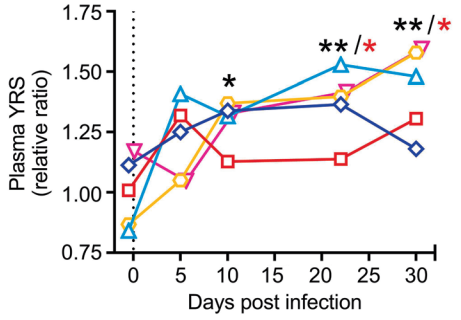

Fig. 6. Increased plasma YRS in Sca1/EGFP Tg mice infected by LCMV-13. Plasma samples were analayzed by ELISA using anti-YRS polyclonal antibodies. Concentrations were calculated from a reference calibration curve of purified recombinant human YRS protein and the results are shown as relative to the average of preinfection value (n = 5). Data were analyzed by RM one-way ANOVA with Dunnett's posttest for multiple comparisons (black asterisks) or nonparametric Friedman test followed by Dunn's posttest (red asterisks). *P < 0.05, **P <0.01.

marker for Sca1 expression. Sca1 (Ly-6A) is a GPI-anchored membrane protein in the *Ly6* gene family, often used as a stem cell marker and likely involved in ligand binding although none is yet known (47). There is no human Sca1 ortholog, but homologs likely exist with functional influence on hematopoietic progenitors (48), immune cells, and tumorigenesis (49). Sca1—an IFN-stimulated gene (50,51)—may help protect HSCs from stress-induced exhaustion, preserving their availability for emergency thrombopoiesis when acute platelet depletion occurs (52,53). Studies of human inflammatory platelets would benefit from identification of Sca1 equivalents, for which reasonable candidates are myeloid markers coexpressed with MK/platelet markers, such as F4/80 and CD42b identified here in Sca1/EGFP$^+$ mouse blood cells. Our immunofluorescence study showed highly adhesive and morphologically distinct features of Sca1/EGFP$^+$ MKs. We speculate that these MKs are directly generated from myeloid/MK-biased HSC, but the exact mechanism of Sca1+ MK generation needs to be elucidated in future studies.

Consistent with the finding that TLR7, a pathogen sensor activated by single-stranded RNA (31,38–40), has a role in the induction of inflammatory platelets, mice infected by LCMV, a single-stranded RNA Arenavirus (41), exhibited profound alterations of thrombopoiesis. Of the viral strains used, LCMV-A causes acute infection cleared in 2–3 wk, while LCMV-13 (only differing in two amino acids) persists >90 d (54,55). As a consequence, IFN-I peak production induced by LCMV-A is ~5 d after infection followed by rapid decline, but in LCMV-13 infection, peak levels are ~4 times higher and production persists for >50 d (56,57). The shutdown of normal Sca1$^-$ platelet production during acute infection with either viral strain is consistent with BM suppression by high IFN-I levels and, in such conditions, generation of inflammatory platelets prevents life-threatening bleeding (42). In LCMV-A acute infection, the rapid restoration of normal Sca1$^-$ platelet counts with symmetrically inverse shutdown of inflammatory Sca1$^+$ platelet generation clearly indicates that the latter is linked to IFNAR signaling. Confirming this, persistent, albeit low-level IFN-I production during recovery from thrombocytopenia in chronic LCVM-13 infection leads to a 50:50 proportion of Sca1 – and + platelets in blood, which is never seen in unperturbed mice. In view of their enhanced adhesive and procoagulant phenotype, defined here, circulating inflammatory platelets beyond emergency response could explain heightened microvascular dysfunction and thrombotic risk in patients with infections, cancer, and metabolic disorders (8,10,58–62).

Untreated mice have no Sca1$^+$ platelets in blood, but nearly equal numbers of Sca1 – and + MKs and progenitors in the BM, consistent with the latter being a quiescent reserve activated only for inflammatory platelet production (53). In the in vivo experiment of WT BM, Sca1$^-$ MKs decrease more and Sca1$^+$ MKs increase less after LPS than GDQ administration; in IFNAR$^{-/-}$ BM, which lacks Sca1$^+$ MKs before or after treatment, Sca1$^-$ MKs decrease after LPS, but not GDQ treatment. Thus, LPS can down-regulate normal MKs independently of IFNAR, but whether this involves TLR4 or a different LPS target remains to be clarified. Thrombocytopenia is frequently observed in patients with sepsis, and the cause of the platelet decrease is explained by multiple mechanisms including enhanced coagulation and platelet consumption (e.g., activation and aggregation). Interestingly, the role of IFN-I in coagulation activation leading to disseminated intravascular coagulation induced by gram-negative bacteria has been reported (63). Thus, IFN-I-mediated inflammatory thrombopoiesis may operate in human sepsis, and alternation in the transcriptional profiles of platelets during sepsis (11) might be, at least partly, explained by inflammatory thrombopoiesis. In support of this idea, ITGA2B encoding integrin αIIb was reported to be up-regulated in platelets of patients with sepsis and was also found to be one of those highly expressed in Sca1/EGFP$^+$ platelets.

In addition to platelets, normal mouse blood contains a small number of CD41$^+$ MKs and precursors, of which ~40 to 60% are Sca1$^+$ reflecting BM distribution. Infection by either LCMV-A or 13 caused, not surprisingly, a sharp decrease in the count of these cells coincident with IFN-I peak production. Of interest, after the acute phase the rebound and return to preinfection counts in blood involved mostly inflammatory Sca1$^+$ MKs and progenitors, which accounted for >80% of total CD41$^+$ cells in blood. This was unexpected, particularly after LCMV-A infection at a time when all platelets in blood were again Sca1$^-$. Relevant to pathobiology, sustained mobilization of myeloid/MK-biased progenitors into the circulation and possibly reaching peripheral tissues can explain enhanced thrombogenicity during infections and chronic inflammatory conditions. These cells may create hypercoagulable conditions leading to microvascular thrombosis, as seen here in

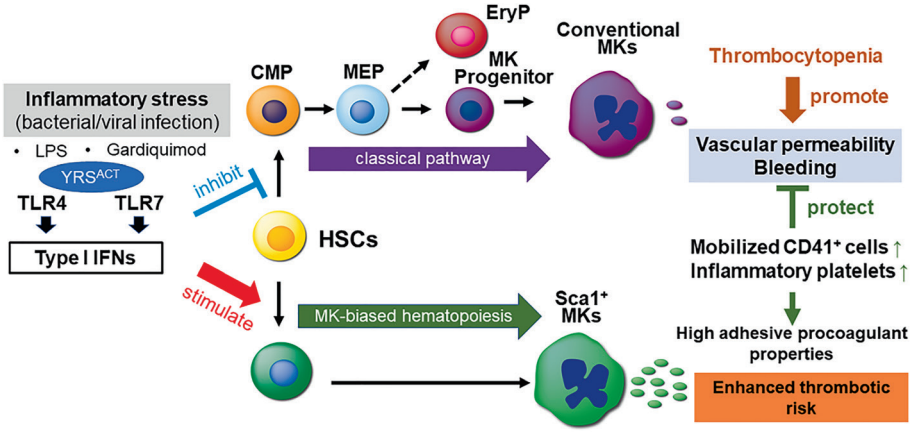

Fig. 7. Schematic representation of inflammatory thrombopoiesis associated with viral infection mimicked by YRS^{ACT}. Inflammatory stress induced by bacterial or viral infection through TLRs, specifically TLR4 and TLR7, induces IFN-I production suppressing normal hematopoiesis and causing thrombocytopenia, but also stimulating inflammatory thrombopoiesis as defense response. Inflammatory platelets and myeloid skewed CD41$^+$ hematopoietic progenitors and MKs released into blood have enhanced adhesive and procoagulant properties, which support endothelial barrier function and hemostasis, but may also have potential to enhance thrombotic risk. Selective stimulation of TLR4 and TLR7 by LPS and Gardiquimod, respectively, and of TLR7 by YRS^{ACT} elicited responses mechanistically similar to infection, but variable in severity. Thus, the induction of IFN-I signaling by distinct pathogen recognition receptors activated by different stimuli may variably change the balance of inhibitory and stimulatory effects on normal and inflammatory thrombopoiesis.

LCMV-infected mice and in sepsis (64). Transcriptional profiling of patients with COVID-19 identified dysregulation of the myeloid lineage with evidence of IFN-I activation and MKs in the circulation (65,66). In addition, the autopsy lungs of critically ill COVID-19 patients and the experimentally infected rhesus macaques have shown microthrombi containing MKs in alveolar capillaries (67–71). These findings are coherent with the viral infection mouse model discussed here.

Alterations of thrombopoiesis dependent on IFNAR signaling occur in the context of innate immune responses downstream of activated TLRs that also involve IFN-I (72). Distinct mechanisms suppress normal platelet production through the MEP pathway (32–35) or induce inflammatory platelet generation from myeloid/MK-biased HSC (17,36), but all converge on one IFNAR receptor. In the model of chronic LCMV-13 infection, persistent IFN-I production leads to concurrent presence of normal and inflammatory platelets in blood. The mechanisms underlying these opposite effects downstream of TLR7 activation are not fully understood, but they clearly allow continued production of phenotypically distinct platelets with enhanced procoagulant/prothrombotic potential, which may turn a host defense response into a disease trigger.

In animal models of inflammation, YRS in blood is increased, indicating a possible role in emergency thrombopoiesis. YRS could also bind transfer RNA (tRNA) or fragments that in turn could activate TLR7 inducing inflammatory thrombopoiesis. Secretion of YRS was shown to be accompanied by site-specific proteolytic cleavage yielding small amounts—relative to native protein present in cytosol– of active YRS fragment (24). In the current study, we could not detect such cleaved YRS due to limited availability of the antibodies with sufficient sensitivities. Previously, using RT-PCR, mRNAs of YRS splice variants encoding key determinants for YRS activity were identified (73,74). One of these variants—N13, expressed in leukocyte, lung, and spleen (74)—skips exon 11 and generates a truncated protein with robust activity in thrombopoiesis similar to YRS^{ACT} (25). It remains to be determined whether inflammatory stress can lead to expression of such variants. Such a concept fits the general hypothesis that many of the alternative functions of aaRSs, only recently uncovered, are deployed during stress insults, including specific diseases (75–79). These concepts establish the mechanistic bases for the use of YRS^{ACT} as a pharmacologic modulator of inflammatory thrombopoiesis to replenish platelets and prevent lethal hemorrhage or vascular leakage.

Materials and Methods

Animal Models. C57BL/6J (WT), Ly6a-EGFP transgenic (Sca1/EGFP), and $IFNAR^{-/-}$ mice were obtained from The Jackson Laboratory. All animal studies were approved by Scripps Research Institutional Animal Care and Usage Committee. Methods for platelet count, BM cell culture, and MK ploidy analysis are found in SI Appendix, Materials and Methods.

Flow Cytometry Analysis. Mouse blood samples were collected from the retro-orbital plexus using sodium citrate as anticoagulant. Blood samples were diluted in PBS (pH 7.4) containing 2 mM EDTA. After blocking Fc receptors with TruStain FcX, samples were stained with anti-CD41, anti-GPIbα (80), or anti-CD11b. DRAQ5 or Hoechst 33342 was used for DNA staining. Samples were analyzed using a Novocyte flow cytometer (ACEA Biosciences). The results were analyzed with FlowJo v.10.7.1. High-dimensional Mass cytometry, imaging flow cytometry, fibrinogen binding analysis, annexin V binding analysis, and MK ploidy analysis are described in SI Appendix, Materials and Methods.

Histological and Immunofluorescence Microscopy Analysis. The harvested mouse organs were snap frozen and cryosectioned. After fixation with 4% paraformaldehyde for 5 min, samples were blocked and permeabilized using 1% Triton X-100 in phosphate-buffered saline (PBS) containing 5% normal goat serum and FcR blocker. Antibodies used for immunostaining are antimouse CD41, anti-CD144, and antifibrin (64C5). The nuclei were counterstained with 4′,6-diamidino-2-phenylindole. For the femur cryosection, the modified Kawamoto film method was employed as previously described (81). Sections were visualized using a BZ-X700 Fluorescence microscope (Keyence) or LSM880 laser scanning confocal microscope (Zeiss), and the images were analyzed and adjusted for contrast using BZ-X Analyzer software or Fiji image analysis software (82).

Statistical Analysis. Data were analyzed using Prism (GraphPad Software, La Jolla, CA) and detailed information is provided in figure legends.

Data, Materials, and Software Availability. All study data are included in the article and/or *SI Appendix*.

ACKNOWLEDGMENTS. This work was supported by National Institutes of Health grants HL129011 (T.K.), HL135294 (Z.M.R.), AI145374 (B.M.S.), GM125908 (P.S.), NS113583 and GM139627 (X.-L.Y.); by fellowships and additional financial support from MERU Foundation (Italy) to Y.M., S.K., A.Z., and T.K.; and by the National Foundation for Cancer Research (S.K., R.S., and T.K.). We thank Yoav Altman (Director, Flow Cytometry Shared Resource at Sanford Burnham Prebys Medical Discovery Institute) for technical support in the analysis of imaging flow cytometry. We would also thank John Shimashita and Steven Head (Genomics Core at Scripps Research) for support in RNA-Seq analysis.

Author affiliations: [a]Department of Molecular Medicine, MERU-Roon Research Center on Vascular Biology, The Scripps Research Institute, La Jolla, CA 92037; [b]The Scripps Laboratories for tRNA Synthetase Research, Department of Molecular Medicine, The Scripps Research Institute, La Jolla, CA 92037; [c]Viral-Immunobiology Laboratory, Department of Immunology and Microbiology, The Scripps Research Institute, La Jolla, CA 92037; [d]MERU-VasImmune, Inc., San Diego, CA 92121; [e]Department of Hematology and Oncology, University of California, San Diego, CA 92093; [f]Rady Children's Hospital, San Diego, CA 92123; [g]Center for Thrombosis and Hemostasis, University Medical Center of the Johannes Gutenberg University, 55128 Germany; and [h]Department of Immunology and Microbiology, The Scripps Research Institute, La Jolla, CA 92037

Author contributions: P.S., Z.M.R., and T.K. designed research; Y.M., S.K., B.M.S., A.Z., J.N.O., E.W., and T.K. performed research; B.M.S., R.S., X.-L.Y., W.R., and P.S. contributed new reagents/analytic tools; Y.M., S.K., P.S., Z.M.R., and T.K. analyzed data; X.-L.Y. advised on experimental design; and S.K., P.S., Z.M.R., and T.K. wrote the paper.

Reviewers: F.I., Rikagaku Kenkyujo; and E.T., University of Oxford.

1. B. Ho-Tin-Noe, Y. Boulaftali, E. Camerer, Platelets and vascular integrity: How platelets prevent bleeding in inflammation. *Blood* **131**, 277–288 (2018).
2. C. N. Morrell, A. A. Aggrey, L. M. Chapman, K. L. Modjeski, Emerging roles for platelets as immune and inflammatory cells. *Blood* **123**, 2759–2767 (2014).
3. D. Projahn, R. R. Koenen, Platelets: Key players in vascular inflammation. *J. Leukoc. Biol.* **92**, 1167–1175 (2012).
4. J. W. Semple, J. Freedman, Platelets and innate immunity. *Cell Mol. Life Sci.* **67**, 499–511 (2010).
5. J. W. Semple, J. E. Italiano Jr., J. Freedman, Platelets and the immune continuum. *Nat. Rev. Immunol.* **11**, 264–274 (2011).
6. M. Iannacone *et al.*, Platelets mediate cytotoxic T lymphocyte-induced liver damage. *Nat. Med.* **11**, 1167–1169 (2005).
7. L. G. Guidotti *et al.*, Immunosurveillance of the liver by intravascular effector CD8(+) T cells. *Cell* **161**, 486–500 (2015).
8. M. Koupenova *et al.*, The role of platelets in mediating a response to human influenza infection. *Nature Commun.* **10**, 1780 (2019).
9. S. R. Clark *et al.*, Platelet TLR4 activates neutrophil extracellular traps to ensnare bacteria in septic blood. *Nat. Med.* **13**, 463–469 (2007).
10. C. Deppermann, P. Kubes, Platelets and infection. *Semin. Immunol.* **28**, 536–545 (2016).
11. E. A. Middleton *et al.*, Sepsis alters the transcriptional and translational landscape of human and murine platelets. *Blood* **134**, 911–923 (2019).
12. R. A. Campbell *et al.*, Human megakaryocytes possess intrinsic antiviral immunity through regulated induction of IFITM3. *Blood* **133**, 2013–2026 (2019).
13. K. R. Machlus, J. E. Italiano Jr, The incredible journey: From megakaryocyte development to platelet formation. *J. Cell Biol.* **201**, 785–796 (2013).
14. N. Debili *et al.*, Characterization of a bipotent erythro-megakaryocytic progenitor in human bone marrow. *Blood* **88**, 1284–1296 (1996).
15. K. Akashi, D. Traver, T. Miyamoto, I. L. Weissman, A clonogenic common myeloid progenitor that gives rise to all myeloid lineages. *Nature* **404**, 193–197 (2000).
16. A. Sanjuan-Pla *et al.*, Platelet-biased stem cells reside at the apex of the haematopoietic stem-cell hierarchy. *Nature* **502**, 232–236 (2013).

17. S. Haas *et al.*, Inflammation-induced emergency megakaryopoiesis driven by hematopoietic stem cell-like megakaryocyte progenitors. *Cell Stem Cell* **17**, 422–434 (2015).
18. S. Pinho *et al.*, Lineage-biased hematopoietic stem cells are regulated by distinct niches. *Dev. Cell* **44**, 634–641.e634 (2018).
19. M. Osawa, K. Hanada, H. Hamada, H. Nakauchi, Long-term lymphohematopoietic reconstitution by a single CD34-low/negative hematopoietic stem cell. *Science* **273**, 242–245 (1996).
20. M. Guo, P. Schimmel, Essential nontranslational functions of tRNA synthetases. *Nat. Chem. Biol.* **9**, 145–153 (2013).
21. S. Kim, S. You, D. Hwang, Aminoacyl-tRNA synthetases and tumorigenesis: More than housekeeping. *Nat. Rev. Cancer* **11**, 708–718 (2011).
22. P. Schimmel, The emerging complexity of the tRNA world: Mammalian tRNAs beyond protein synthesis. *Nat. Rev. Mol. Cell Biol.* **19**, 45–58 (2018).
23. M. Guo, X. L. Yang, P. Schimmel, New functions of aminoacyl-tRNA synthetases beyond translation. *Nat. Rev. Mol. Cell Biol.* **11**, 668–674 (2010).
24. K. Wakasugi, P. Schimmel, Two distinct cytokines released from a human aminoacyl-tRNA synthetase. *Science* **284**, 147–151 (1999).
25. T. Kanaji *et al.*, Tyrosyl-tRNA synthetase stimulates thrombopoietin-independent hematopoiesis accelerating recovery from thrombocytopenia. *Proc. Natl. Acad. Sci. U.S.A.* **115**, E8228–E8235 (2018).
26. E. Won *et al.*, Extracellular tyrosyl-tRNA synthetase cleaved by plasma proteinases and stored in platelet α-granules: Potential role in monocyte activation. *Res. Pract. Thromb. Haemost.* **4**, 1167–1177 (2020).
27. X. Ma, C. Robin, K. Ottersbach, E. Dzierzak, The Ly-6A (Sca-1) GFP transgene is expressed in all adult mouse hematopoietic stem cells. *Stem Cells* **20**, 514–521 (2002).
28. L. Van der Maaten, G. Hinton, Visualizing Data using t-SNE. *J. Mach. Learn. Res* **9**, 2579–S2605 (2008).
29. S. I. Miller, R. K. Ernst, M. W. Bader, LPS, TLR4 and infectious disease diversity. *Nat. Rev. Microbiol.* **3**, 36–46 (2005).
30. M. Buitendijk, S. K. Eszterhas, A. L. Howell, Gardiquimod: A Toll-like receptor-7 agonist that inhibits HIV type 1 infection of human macrophages and activated T cells. *AIDS Res. Hum. Retroviruses* **29**, 907–918 (2013).
31. K. Crozat, B. Beutler, TLR7: A new sensor of viral infection. *Proc. Natl. Acad. Sci. U.S.A.* **101**, 6835–6836 (2004).
32. L. H. Wang, R. J. Kulmacz, Thromboxane synthase: Structure and function of protein and gene. *Prostaglandins Other Lipid. Mediat.* **68–69**, 409–422 (2002).
33. D. Binder, J. Fehr, H. Hengartner, R. M. Zinkernagel, Virus-induced transient bone marrow aplasia: Major role of interferon-alpha/beta during acute infection with the noncytopathic lymphocytic choriomeningitis virus. *J. Exp. Med.* **185**, 517–530 (1997).
34. A. Verma *et al.*, Activation of the p38 mitogen-activated protein kinase mediates the suppressive effects of type I interferons and transforming growth factor-beta on normal hematopoiesis. *J. Biol. Chem.* **277**, 7726–7735 (2002).
35. A. Yamane *et al.*, Interferon-α2b-induced thrombocytopenia is caused by inhibition of platelet production but not proliferation and endomitosis in human megakaryocytes. *Blood* **112**, 542–550 (2008).
36. M. A. Essers *et al.*, IFNalpha activates dormant haematopoietic stem cells in vivo. *Nature* **458**, 904–908 (2009).
37. R. K. Andrews *et al.*, A novel viper venom metalloproteinase, alborhagin, is an agonist at the platelet collagen receptor GPVI. *J. Biol. Chem.* **276**, 28092–28097 (2001).
38. J. M. Lund *et al.*, Recognition of single-stranded RNA viruses by toll-like receptor 7. *Proc. Natl. Acad. Sci. U.S.A.* **101**, 5598–5603 (2004).
39. F. Heil *et al.*, Species-specific recognition of single-stranded RNA via toll-like receptor 7 and 8. *Science* **303**, 1526–1529 (2004).
40. S. S. Diebold, T. Kaisho, H. Hemmi, S. Akira, C. Reis e Sousa, Innate antiviral responses by means of TLR7-mediated recognition of single-stranded RNA. *Science* **303**, 1529–1531 (2004).
41. J. C. de la Torre, Molecular and cell biology of the prototypic arenavirus LCMV: Implications for understanding and combating hemorrhagic fever arenaviruses. *Ann. N. Y. Acad. Sci.* **1171**, E57–E64 (2009).
42. R. Aiolfi *et al.*, Arenaviral infection causes bleeding in mice due to reduced serotonin release from platelets. *Sci. Signal* **15**, eabb0384 (2022).
43. N. R. Emambokus, J. Frampton, The glycoprotein IIb molecule is expressed on early murine hematopoietic progenitors and regulates their numbers in sites of hematopoiesis. *Immunity* **19**, 33–45 (2003).
44. M. T. Mitjavila-Garcia *et al.*, Expression of CD41 on hematopoietic progenitors derived from embryonic hematopoietic cells. *Development* **129**, 2003–2013 (2002).
45. C. Gekas, T. Graf, CD41 expression marks myeloid-biased adult hematopoietic stem cells and increases with age. *Blood* **121**, 4463–4472 (2013).
46. K. Wakasugi, P. Schimmel, Highly differentiated motifs responsible for two cytokine activities of a split human tRNA synthetase. *J. Biol. Chem.* **274**, 23155–23159 (1999).
47. C. Holmes, W. L. Stanford, Concise review: Stem cell antigen-1: Expression, function, and enigma. *Stem Cells* **25**, 1339–1347 (2007).
48. S. B. Bradfute, T. A. Graubert, M. A. Goodell, Roles of Sca-1 in hematopoietic stem/progenitor cell function. *Exp. Hematol.* **33**, 836–843 (2005).
49. G. Upadhyay, Emerging role of lymphocyte antigen-6 family of genes in cancer and immune cells. *Front. Immunol.* **10**, 819 (2019).
50. E. M. Pietras *et al.*, Re-entry into quiescence protects hematopoietic stem cells from the killing effect of chronic exposure to type I interferons. *J. Exp. Med.* **211**, 245–262 (2014).
51. M. Kanayama *et al.*, CD86-based analysis enables observation of bona fide hematopoietic responses. *Blood* **136**, 1144–1154 (2020).
52. S. Zhang *et al.*, Expansion of quiescent hematopoietic stem cells under stress and nonstress conditions in mice. *Stem Cell Rev. Rep.* **18**, 2388–2402 (2022), 10.1007/s12015-022-10380-6.
53. S. Singh, B. Jakubison, J. R. Keller, Protection of hematopoietic stem cells from stress-induced exhaustion and aging. *Curr. Opin. Hematol.* **27**, 225–231 (2020).
54. B. M. Sullivan *et al.*, Point mutation in the glycoprotein of lymphocytic choriomeningitis virus is necessary for receptor binding, dendritic cell infection, and long-term persistence. *Proc. Natl. Acad. Sci. U.S.A.* **108**, 2969–2974 (2011).
55. M. B. A. Oldstone *et al.*, Lymphocytic choriomeningitis virus Clone 13 infection causes either persistence or acute death dependent on IFN-1, cytotoxic T lymphocytes (CTLs), and host genetics. *Proc. Natl. Acad. Sci. U.S.A.* **115**, E7814–E7823 (2018).
56. J. R. Teijaro *et al.*, Persistent LCMV infection is controlled by blockade of type I interferon signaling. *Science* **340**, 207–211 (2013).
57. B. Hahm, M. J. Trifilo, E. I. Zuniga, M. B. Oldstone, Viruses evade the immune system through type I interferon-mediated STAT2-dependent, but STAT1-independent, signaling. *Immunity* **22**, 247–257 (2005).
58. K. Y. Stokes, D. N. Granger, Platelets: A critical link between inflammation and microvascular dysfunction. *J. Physiol.* **590**, 1023–1034 (2012).
59. D. D. Wagner, P. C. Burger, Platelets in inflammation and thrombosis. *Arterioscler. Thromb. Vasc. Biol.* **23**, 2131–2137 (2003).
60. J. R. Hitchcock *et al.*, Inflammation drives thrombosis after Salmonella infection via CLEC-2 on platelets. *J. Clin. Invest.* **125**, 4429–4446 (2015).
61. W. Zheng, H. Zhang, D. Zhao, J. Zhang, J. W. Pollard, Lung mammary metastases but not primary tumors induce accumulation of atypical large platelets and their chemokine expression. *Cell Rep.* **29**, 1747–1755.e1744 (2019).
62. M. Gawaz, H. Langer, A. E. May, Platelets in inflammation and atherogenesis. *J. Clin. Invest.* **115**, 3378–3384 (2005).
63. X. Yang *et al.*, The role of type 1 interferons in coagulation induced by gram-negative bacteria. *Blood* **135**, 1087–1100 (2020).
64. C. Garcia *et al.*, Platelet versus megakaryocyte: Who is the real bandleader of thromboinflammation in sepsis? *Cells* **11**, 1507 (2022).
65. J. Schulte-Schrepping *et al.*, Severe COVID-19 is marked by a dysregulated myeloid cell compartment. *Cell* **182**, 1419–1440.e1423 (2020).
66. J. R. Jones, R. Ireland, Morphological changes in a case of SARS-CoV-2 infection. *Blood* **135**, 2324 (2020).
67. A. Nunes Duarte-Neto *et al.*, Pulmonary and systemic involvement of COVID-19 assessed by ultrasound-guided minimally invasive autopsy. *Histopathology* **77**, 186–197 (2020), 10.1111/his.14160.
68. S. E. Fox *et al.*, Pulmonary and cardiac pathology in African American patients with COVID-19: An autopsy series from New Orleans. *Lancet Respir. Med.* **8**, 681–686 (2020), 10.1016/s2213-2600(20)30243-5.
69. L. Carsana *et al.*, Pulmonary post-mortem findings in a series of COVID-19 cases from northern Italy: A two-centre descriptive study. *Lancet Infect. Dis.* **20**, 1135–1140 (2020).
70. L. Roncati *et al.*, A proof of evidence supporting abnormal immunothrombosis in severe COVID-19: Naked megakaryocyte nuclei increase in the bone marrow and lungs of critically ill patients. *Platelets* **31**, 1085–1089 (2020).
71. M. Aid *et al.*, Vascular disease and thrombosis in SARS-CoV-2-infected rhesus macaques. *Cell* **183**, 1354–1366.e13 (2020), 10.1016/j.cell.2020.10.005.
72. A. M. Green, P. R. Beatty, A. Hadjilaou, E. Harris, Innate immunity to dengue virus infection and subversion of antiviral responses. *J. Mol. Biol.* **426**, 1148–1160 (2014).
73. Z. Wei *et al.*, Alternative splicing creates two new architectures for human tyrosyl-tRNA synthetase. *Nucleic Acids Res.* **44**, 1247–1255 (2016).
74. W. S. Lo *et al.*, Human tRNA synthetase catalytic nulls with diverse functions. *Science* **345**, 328–332 (2014).
75. N. Wei *et al.*, Oxidative stress diverts tRNA synthetase to nucleus for protection against DNA damage. *Mol. Cell* **56**, 323–332 (2014).
76. S. Bervoets *et al.*, Transcriptional dysregulation by a nucleus-localized aminoacyl-tRNA synthetase associated with Charcot-Marie-Tooth neuropathy. *Nat. Commun.* **10**, 5045 (2019).
77. M. C. Park *et al.*, Secreted human glycyl-tRNA synthetase implicated in defense against ERK-activated tumorigenesis. *Proc. Natl. Acad. Sci. U.S.A.* **109**, E640–E647 (2012).
78. Y. H. Ahn *et al.*, Secreted tryptophanyl-tRNA synthetase as a primary defence system against infection. *Nat. Microbiol.* **2**, 16191 (2016).
79. T. F. Williams, A. C. Mirando, B. Wilkinson, C. S. Francklyn, K. M. Lounsbury, Secreted Threonyl-tRNA synthetase stimulates endothelial cell migration and angiogenesis. *Sci. Rep.* **3**, 1317 (2013).
80. N. Yokota *et al.*, Contributions of thrombin targets to tissue factor-dependent metastasis in hyperthrombotic mice. *J. Thromb. Haemost.* **12**, 71–81 (2014).
81. Y. Morodomi, S. Kanaji, E. Won, T. Kawamoto, T. Kanaji, Modified application of Kawamoto's film method for super-resolution imaging of megakaryocytes in undecalcified bone marrow. *Res. Pract. Thromb. Haemost.* **4**, 86–91 (2020).
82. J. Schindelin *et al.*, Fiji: An open-source platform for biological-image analysis. *Nat. Met.* **9**, 676–682 (2012).